Physical Model of a Weld Bead Deposit on an Inclined or Horizontal Support Applied for Wire and Arc Additive Manufacturing

Chetra Mang, Xavier Lorang, Ramdane Tami, François Rouchon

Physical model of a weld bead deposit on an inclined or horizontal support applied for wire and arc additive manufacturing

Chetra Mang[1*], Xavier Lorang[1], Ramdane Tami[1], and François Rouchon[1,2]

[1] Institut de Recherche Technologique SystemX, 2 Bd Thomas Gobert, 91120 Palaiseau,
chetra.mang@irt-systemx.fr
xavier.lorang@irt-systemx.fr
ramdane.tami@irt-systemx.fr
francois.rouchon@irt-systemx.fr
[2] Université Paris-Saclay, ENS Paris-Saclay, LURPA, 91190 Gif-sur-Yvette, France

Keywords: *Wire and arc additive manufacturing, Young-Laplace equation, Bead topology, Electro-mechanical power generator*

Abstract. *The present work is carried out in the framework of the WAS project [1] which deals with the WAAM process. The process relies on an automatized welding process in which a part is built by a successively deposed metal bead. Under a two-dimensional hypothesis, we propose a physically based bead topology model using the equilibrium between the hydrostatic pressure and the capillarity force. This equilibrium can be described by the Young-Laplace equation [2]. The proposed model can also estimate a bead topology that is deposed on a horizontal or inclined support. To do so, the Young equation is used to balance the forces at the tri-phase point [3]. Moreover, the bead topology model requires a deposed melted metal volume. By modeling a gas metal arc welding (GMAW) power generator system [4], the volume can be estimated and used as a physical parameter for the bead topology model. Combining the topology and the power generator models, the resulting synergy enables to simulate the topology of a weld bead of a WAAM process. In addition to the modelling, experimental profiles of the beads are used to validate the model.*

1 INTRODUCTION

In recent years, metal additive manufacturing (MAM) has grown with very strong interest in academic research and industrial applications. Among MAM processes, wire and arc additive manufacturing (WAAM) became very popular through its advantages in the manufacturing medium and large-scale components [5]. Even though, the manufacturability of a part relies on manufacturing topology because the part's geometry defects such as planarity defect can induce the collision between the welding torch and the part or the part's geometry deviation from the targeted geometry. This defect is linked to the process parameters such as the synergy of power generator: wire-speed vs current and voltage and the robot parameters: trajectory and torch speed. To avoid these defects, one needs to be capable of simulating the topology of the manufacturing part by the weld bead deposition. Thus, it is necessary to be able to simulate the topology of a weld bead. Primarily, the topology of a weld bead is depending on the deposed wire feed volume. One needs to be able to correctly estimate the deposed volume from the wire feed via the power generator. Consequently, the power generator model is required to do so. A dynamic model of drops detaching from a gas metal arc welding electrode has been proposed [6]. The model allows determining the kinematics of the drops as well as the wire speed, the

current, and the voltage of the welding arc. The model is simplified in this study to only simulate the wire speed to estimate the deposed volume of a weld bead.

According to the welding process, the wire feed is melting and many drops of the metal liquid form a molten pool. A weld bead is formed by consecutive deposition of the molten pool. In the liquid state, the molten pool forms a disc section at the equilibrium by the capillary and gravity forces. During the solidification of the pool, the temperature at the deposed zone directly affects the geometry of the pool. The temperature is linked directly to the heat supply from the melting wire feed. When the wire feed speed is very slow, the heat supply is very low. Thus, the weld bead geometry is stick out because there is not sufficient energy to melt the substrate at the deposed zone. Otherwise, when the wire feed speed is very fast, the heat supply is very high. Thus, the weld bead geometry is flat. In order to obtain a weld bead geometry at solidification approximated to that of the molten pool, the wire feed speed should be sufficiently large to obtain the necessary heat supply to melt the deposed zone. Moreover, the temperature of the deposed zone should not be too high to assure a good grip of the weld bead on the deposed zone. The good temperature of the deposed zone is estimated to be between 80° and 150° to assure the good grip of the weld bead and the substrate [7].

With a good heat supply and a good temperature on a deposed zone, the weld bead section geometry can be approximated to a circular arc. [8] has proposed a weld bead deposition using the Laplace equation by the 2D prismatic assumption to simulate a 2D profile of a weld bead. However, to be able to simulate the profile, the model parameters (contact angle and curvature) need to be estimated from the experimental profiles according to the process parameters. The weld bead deposition is assumed to be deposed either on a horizontal plane or another weld bead in a single column symmetrically. To overcome the estimation of the contact angle by experimental profiles, [3] has proposed a thermo-dynamical equilibrium of a drop with a given volume to determine the contact angle on convex or concave support with symmetrical deposition. When a hysteretic contact angle occurs, the equilibrium is no longer satisfied. On the other hand, [9] has used a state equation to determine the surface tension forces of the tri-phases using different drop volumes. In the study, on the other hand, the state equation is used to couple with the Laplace equation to determine the contact angle and build the 2D weld bead profile with different area sections. The state equation parameters are calibrated with two experimental profiles.

Physically, when the drop profile is symmetric on the support, either the thermo-dynamical or the state equation can be used to determine the contact angle of the drop profile. But, when the support is in an inclined position, the drop could lose its equilibrium and falls along the support. However, if the drop is in equilibrium, the hysteretic contact angle occurs. The advance and recession contact angles of the drop appear. [10] has proposed the equilibrium condition of a water drop with a given volume on an inclined plane with a hysteretic contact angle. The equilibrium condition is used to verify whether the drop is in equilibrium on an inclined plane. For a given inclined plane, the author has determined the critical volume at which the drop loses its equilibrium. On the other hand, in the study, we use the same equilibrium condition under 2D assumption coupling with the Laplace equation to build a weld bead 2D profile on an inclined plane.

2 METHODOLOGIES

To simulate a weld bead topology according to the WAAM process, the volume of a deposed weld bead needs to be correctly estimated. The volume can be computed by the matter flow from the feed wire, hence the feed wire speed. The wire speed is a synergy parameter related directly to the current and the voltage of power generator. The wire speed can be varied depending on the welding process employed. For example, in the Cold Metal Transfer (CMT – Fronius [11]) welding process, to stabilize some parameters, the wire-speed evolves during the welding of a weld bead, on the other hand, in the pulsed welding process, the wire speed remains unchanged. This work proposes a simplified power generator model of the CMT welding process to simulate the wire speed. Then, the wire speed is used to estimate the deposed weld bead area section considering the shrinkage solidification. After that, the estimated area section is used to feed the topology model to simulate the weld bead profile on an inclined or a horizontal plane. The following subsections describe a power source model for the CMT welding process, a method for numerically measuring the contact angle, a method for determining the shrinkage value, and topology models for weld bead deposition on an inclined and a horizontal plane.

2.1 Electro-mechanical power source model

In WAAM process technology, the CMT welding process, which has been introduced by Fronius [11], has been used to manufacture the weld beads considered in this work. This process is an evolution of the Metal Inert Gas and Metal Active Gas (MIG-MAG) welding process with short-circuit transfer regime, in which the electrical signal wave shape and wire supply system are controlled. More specifically, the arc-length (l_{arc}) control method is introduced to stabilize the arc-length, minimize the energy consumption and reduce the deposition projection [12].

Fig. 1 illustrates a system used to simulate and reproduce the CMT process behavior. The power generator produces a constant voltage to feed the electrical circuit such that the wire is an electrode and the substrate an anode. The given synergy of wire feed speed and voltage of the power generator is applied to the system. As shown in figure 1., Contact Tube Welding Distance (CTWD), in short, CT is an external parameter that influences the resultant current and arc voltage wave shapes. As consequence, it impacts also the wire speed. This change in wire speed allows stabilizing the targeted arc-length.

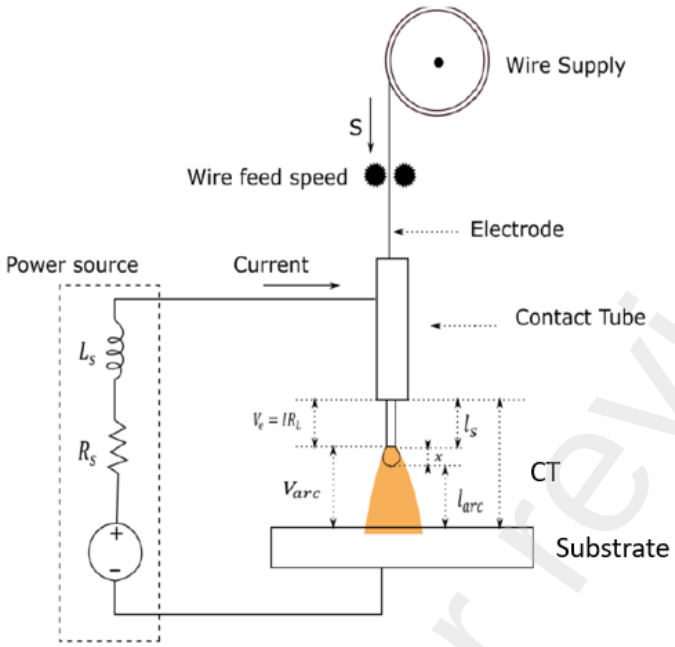

Figure 1: Welding circuit model.

The depicted system is described by a system of physical equations such as the dynamic of the current (I), the arc tension (V_{arc}), the molten wire flow (M_r), and the dynamic of the stick-out length (l_s) [6] as follows:

$$\begin{cases} \dfrac{dI}{dt} = \dfrac{V_{oc} - R_l I - V_{arc} - R_s I}{L_s} \\ V_{arc} = V_0 + R_a I + E_a(CT - l_s) \\ M_r = C_1 I + C_2 \phi l_s I^2 \\ \dfrac{dl_s}{dt} = ws - \dfrac{M_r}{\pi r_w^2} \end{cases} \quad (1)$$

Where:
V_{oc} is the voltage of the power generator;
R_l is electrode resistance;
R_s is the equivalent resistance of the power generator;
L_s is the equivalent inductance power source;
V_0 is arc voltage constant;
R_a is arc resistance;
E_a is arc-length factor;

ϕ is electrode resistivity;
C_1, C_2 are fusion flow constants;
ws is initial wire speed;
r_w is wire radius.

Equation (1) can be written as shown in [6] as follows:

$$\begin{cases} R_l = \phi\left(l_s + \dfrac{r_d + x_1}{2}\right) \\ \dfrac{dl_s}{dt} = ws - \dfrac{M_r}{\pi r_w^2} \\ \dfrac{dI}{dt} = \dfrac{V_{oc} - (R_a + R_s + R_l)I - V_0 - E_a(CT - l_s)}{L_s} \end{cases} \quad (2)$$

Where
x_1 is the displacement of the drop;
r_d is the drop radius;

As previously mentioned, we are only interested in wire speed to determine the molten pool volume for physical topology simulation. Moreover, the drop radius and displacement are very small compared to the stick-out length, thus $R_l \approx \phi l_s$. Equation (2) can be simplified as follows:

$$\begin{cases} \dfrac{dl_s}{dt} = ws - \dfrac{C_1 I + C_2 \phi l_s I^2}{\pi r_w^2} \\ \dfrac{dI}{dt} = \dfrac{V_{oc} - (R_a + R_s + \phi l_s)I - V_0 - E_a(CT - l_s)}{L_s} \end{cases} \quad (4)$$

Equation (4) allows solving for the resultant current and wire speed. The required inputs for the system are power source voltage (V_{oc}) , initial wire-speed (ws), contact tube welding distance (CT), and wire radius (r_w). The fusion flow constant parameters have a direct impact on the molten flow. Hence, these constants are dependent directly on the synergy of weld bead deposition. These parameters are needed to be identified by calibration of the system and the experimental measures. Other parameters are chosen according to steel properties as shown in table 1.

Table 1: Parameters of the power source model of the steel material.

$R_s(m\Omega)$	$L_s(\mu H)$	$V_0(V)$	$R_a(m\Omega)$	$E_a(V/m)$	$\phi(\Omega/m)$
75	20	15.7	4	1500	0.13

To calibrate the fusion flow constant parameters C_1 and C_2, we need to manufacture a weld bead for given synergy process parameters V_{oc}, r_w, ws and CT. For a given value of CT, the measured wire speed is extracted from the experiment. The mean value of experiment wire speed (ws_{meas}) over a straight deposed weld bead is then computed. From equation (2), we can express the mean value of simulation wire-speed in function of C_1 and C_2: $ws_{sim}(C_1,C_2)$. We can find the optimal fusion flow constants as follows:

$$(C_1^*,C_2^*) = argmin(|ws_{sim}(C_1,C_2) - ws_{meas}|) \quad (5)$$

The calibration and validation of the model are carried out on an experiment of a weld bead manufacturing with three different values of contact tube welding distance $CT = 10, 15$, and $20\ mm$. The results are shown in the discussion section.

2.2 Physical topology model

We focused, in this study, on topology models of a weld bead deposed on a horizontal plane and an inclined plane. Weld bead topology can be described by the Laplace equation of drop's hydrostatic pressure and capillary force equilibrium, but at the tri-phase line, the equation cannot overcome the determination of the contact angle. The Young equation is necessary to determine the contact angle at the line. In the following sections, we describe the 2D Laplace weld bead profile, a method to compute the contact angle, a method to estimate the shrinkage value and geometrical models for a weld bead deposed on an inclined and a horizontal plane.

2.2.1 Laplace weld bead profile

Molten pool under the electrical arc can be acted by several kinds of forces such as Lorentz force, buoyance force, arc shear stress, and surface tension force [8]. By considering these forces, the molten pool topology can have a very complicated shape. Under the 2D hypothesis as in [13], it is stated that the approximated topology of the molten pool can be handled by a static liquid state which is the equilibrium between the hydrostatic pressure and the capillarity force. This equilibrium can be expressed as the Laplace equation:

$$\Delta P = \gamma C \quad (6)$$

By assuming that the curvature radius is isotropic, we can write the equation in 2D as follows:

$$0.5\kappa^{-2}z^2 - C_0 z + 2\left(\frac{\frac{dx}{dz}}{\sqrt{1 + \left(\frac{dx}{dz}\right)^2}} - 1\right) = 0 \tag{7}$$

or

$$\begin{cases} \dfrac{dx}{dz} = \dfrac{1}{\tan(\theta_0)} \\ 0.5\kappa^{-2}z^2 - C_0 z = 2(\cos(\theta_0) - 1) \end{cases} \tag{8}$$

Where θ_0 is Laplace contact angle illustrated in fig. 2 which is formed by a tangent to the contact point of the Laplace profile and the horizontal line;

C_0 is the curvature at point P_0 $(x = 0,\ z = 0)$ the origin of the local reference frame (Oxz);

$\kappa = \sqrt{\frac{\gamma}{\rho g}}$ is the capillary length;

γ is the surface tension force between liquid-vapor surface;

g is the gravity;

ρ_m is the metal density at temperature T_m (melting temperature of the metal);

In this work, steel material is considered with the following values: $\gamma = 1.8N/m$,$\rho = 7150kg/m^3$ and $g = 9.8m/s^2$.

As shown in fig. 2, the topology of the drop at equilibrium can be built by the equation depending on the position of the local reference frame at $(x = 0,\ z = 0)$. There are two different positions of local reference frame origin, for example, the origin P_0 or $P_0{}'$ which can be chosen depending on the normal direction of the support (up or down).

The above equation can be solved numerically by the finite difference method or analytically by the elliptic function of the first and second kinds. As illustrated in fig. 3, the solution of the numerical method is in good agreement with the analytical one. However, the computational time of the numerical method is only 0.02 s which is 15 times faster than the analytical one which is 0.3 s.

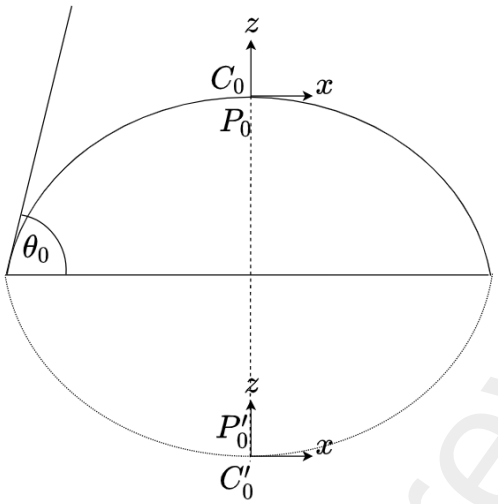

Figure 2: 2D weld bead profile scheme.

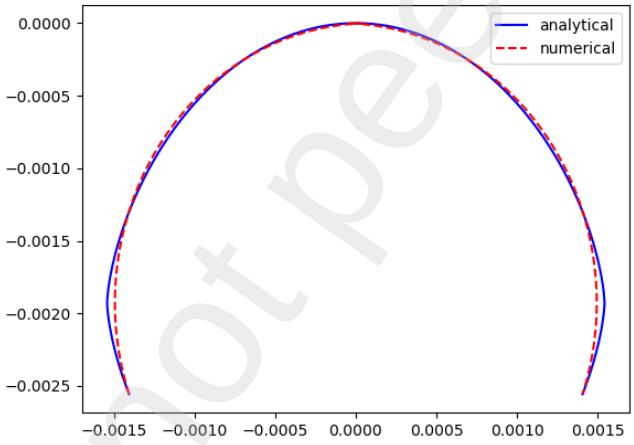

Figure 3: Comparison of the numerical and analytical solutions of 2D Laplace equation.

2.2.2 Contact angle measurement

The contact angle is defined as a tangential angle to the weld bead topology at the support. This angle is formed by the equilibrium at the tri-phase line which is the intersection of liquid, gas, and solid.

While a drop is in an equilibrium state, the drop topology satisfies the Young Laplace equation. For the 2D hypothesis, the shape of the drop is much closed to a circular arc. As a consequence, using circular shape to better fit the form of the drop is the best alternative. However, at a configuration in which the contact angle is larger than $\frac{\pi}{2}$, the circle fitting method can numerically generate an error. Therefore, a polynomial correction is necessary in this case.

This method has been proposed in [14].

Fig. 4 (a) displays a photo of a weld bead specimen, (b) a 3D cloud point of the center part of the weld bead, and (c) the experimental fit profile of the 2D projection of the cloud point along its axis. Because the scan of the cloud points is in low-resolution quality, the precise contact angle cannot be measured. It requires to focus in section profile which represents the circular arc to fit with the Laplace 2D profile as shown in Fig. 5 (a). Fig. 5 (b) depicts the mentioned contact angle measurement method.

The proposed method is used to numerically estimate the contact angles for all the specimens in this study to validate the contact angle of the proposed topology model.

(a)

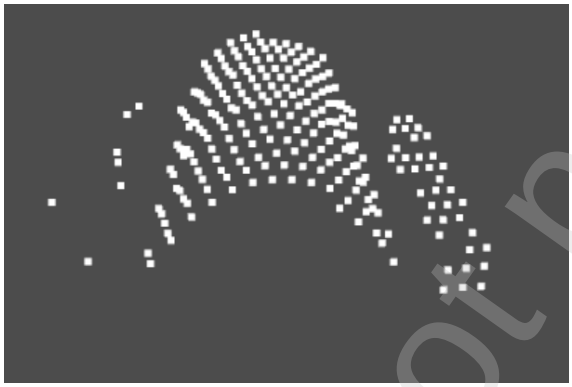

(b)

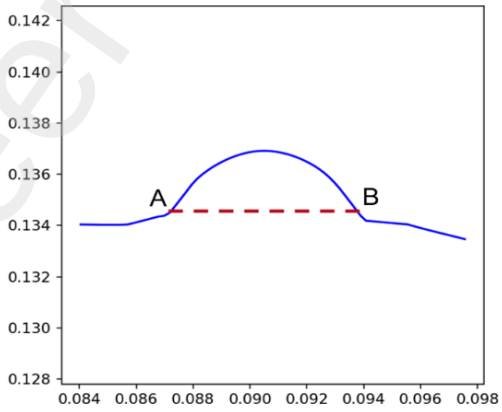

(c)

Figure 4: (a) weld bead picture, (b) cloud point at the center part of the weld bead, and (c) 2D experimental profile of the weld bead associated with the cloud point.

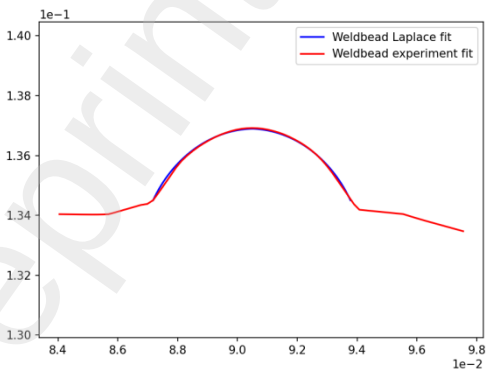

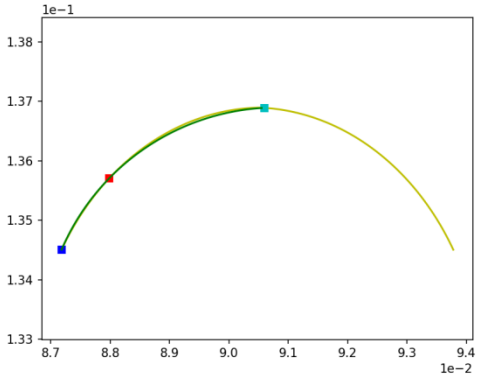

(a) (b)

Figure 5: (a) Laplace profile fitted to the experimental profile and (b) contact angle measurement by circle arc fitting.

2.2.3 Solidification shrinkage

Welding induces high localized temperature and causes the metal molten. This non-uniform change of temperature induces non-uniform stresses because of the expansion and contraction of the heated metal. At the heat-affected zone (HAZ) around the molten pool, due to the thermal expansion, compressive stresses occur at cold parent metal and on the other hand, the tensile stresses at the same point occur when the molten pool is cooled down, which creates the thermal contraction at the HAZ. The change in thermal stresses can be observed by the volume change in the welded zone. More specifically, the volume change is called solidification shrinkage. This change follows three consecutive phases [15]:

- Shrinkage of the liquid metal when lowering the temperature at the liquid state;
- Shrinkage during the solidification at the freezing temperature passing from the liquid state to the solid-state;
- Shrinkage of the solid metal from the freezing temperature to the lower one.

For a given metal, in the first phase, the shrinkage value is fixed, but, in the last one, it strongly varies depending on the thermal stresses in the HAZ [15]. For the first two phases, the shrinkage of the steel is around 3% and for the last phases, the shrinkage varies and is about 7% [16].

This section is dedicated to the evaluation of shrinkage value. Fig. 6 (a) displays the mesh of the scan of a weld bead which is produced by three different CT: $10, 15$ and 20 mm consecutively. Firstly, parts 1, 2 and 3 are chosen to be the post-processing zones. This figure shows that when CT is larger, the sectional area deposition is also larger. With a quantitative value of these three sectional area depositions, the shrinkage is computed based on flow from the wire speed $d_{wire} = \frac{\int_{t_0}^{t_0+\Delta t} ws(t)dt}{\Delta t}$ and the torch speed $d_{bead} = \frac{\Delta V \times v_r}{\Delta L}$ where ws is instant measured wire speed, Δt is the time interval in which torch travel with distance ΔL with the deposed volume of the weld bead ΔV, and v_r is torch speed. The shrinkage is computed by $s = \frac{|d_{bead} - d_{wire}|}{d_{wire}}$. Thus, the weld bead area section $A = (1 - s)A_s$ where $A_s = \frac{\pi r^2 ws}{v_r}$. We identify the overall shrinkage value by its maximum value of the three parts which is used to identify the weld bead area section in the following sections by simulating the power source model to obtain simulated wire-speed. The obtained value of wire-speed s is illustrated in table 2.

Table 2: The wire speed feed and of the weld bead by the torch speed and the shrinkage computation of the three parts of the weld bead.

	Part 1 CT = 20 mm	Part 2 CT=15mm	Part 3 CT=10 mm	s_{max}
$d_{bead}(10^{-7}m^3)$	1.337	1.218	1.092	
$d_{wire}(10^{-7}m^3)$	1.356	1.320	1.193	
s	0.014	0.077	0.084	0.084

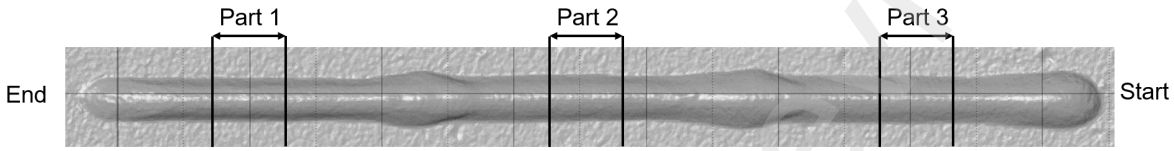

Figure 6: Mesh of the scan of the weld bead with the three parts of CT=10, 15, 20 mm.

2.2.4 Inclined plane deposition

A liquid drop is equilibrated on an inclined plane due to the occurrence of the hysteretic contact angle [2]. This angle is defined by the difference between the advanced contact angle (θ_a) and the recession contact angle (θ_r) of a drop on an inclined plane of angle α as shown in fig. 7. Guéré [10] has demonstrated a method to determine the equilibrium condition of a known volume of water drop on an inclined plane.

The surface tension force $f_p = l\gamma\big(\cos(\theta_r) - \cos(\theta_a)\big)$ at the tri-phase line is balanced with gravity force $f_g = \rho g \Omega \sin(\alpha)$ where l is the tri-phase line length, ρ is the density of the liquid, Ω is the volume of the liquid, g is the gravity constant. The equilibrium condition is satisfied when $f_p \geq f_g$.

In the case of weld bead deposition, a molten pool is formed by the deposition of a mount of metal liquid drops. The volume of the molten pool is very difficult to estimate. According to the 2D topology profile, a sectional area can be correctly computed. To simplify the volume estimation, we suppose that $l \approx \Omega/A$ where A is the sectional area of the weld bead. We can express tension force per unit length as $f_p^l \approx \gamma \Delta\theta \sin(\theta)$ where hysteretic contact angle $\Delta\theta = \theta_a - \theta_r$ and mean contact angle $\theta = \frac{\theta_a + \theta_r}{2}$ and gravity per unit length $f_g^l = \rho g A sin(\alpha)$. The equilibrium condition can be written as $f_p^l \geq f_g^l$.To construct a complete profile of 2D topology weld bead on an inclined plane, we can solve the following system of the equation:

$$\begin{cases} \dfrac{dx}{dz} = \dfrac{1}{\tan(\theta_0)} \\ 0.5\kappa^{-2}z^2 - C_0 z = 2(\cos(\theta_0) - 1) \\ A(f)(C_0) = A \\ \gamma\Delta\theta\sin(\theta) = \rho g A sin(\alpha) \end{cases} \quad (9)$$

Where f is the Laplace profile of the weld bead;

We solve the system step by step as follows:

- First, solving for the Laplace profile f for a given θ_0 and C_0 by the first two equations of the equation system (9);
- Second, with the Laplace profile, solving for C_0 to satisfy the third equation of the equation system (9);
- Third, solving for θ_0 such that the last equation of the equation system (9) is satisfied. The angle can be called the critical Laplace contact angle;

The validation of the proposed simulation of the weld bead deposition strategy on an inclined plane will be performed according to experimental specimen manufactured with different inclined angles. The results are illustrated in the discussion section.

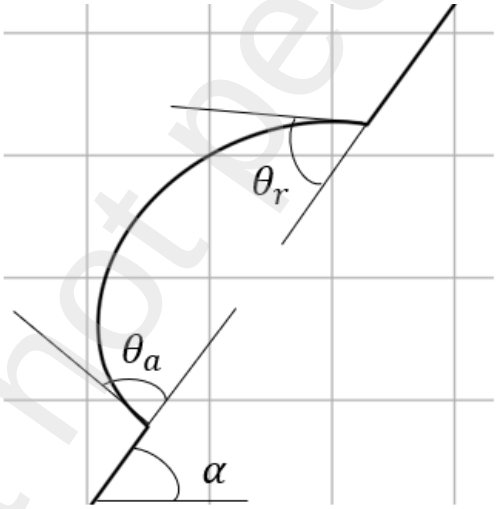

Figure 7: A weld bead on an inclined plane with advance and recession contact angles.

2.2.5 Horizontal plane deposition

When a weld bead is deposed on a horizontal plane, a hysteretic contact angle doesn't appear. In this case, the global equilibrium cannot be used. To determine the contact angle, we can only use the Young equation for the equilibrium at the tri-phase line [3]:

$$\begin{cases} A_{sl} = \gamma_{sv} + \gamma_{lv} - \gamma_{sl} \\ A_{sl} = \gamma_{lv}(1 + \cos(\theta)) \end{cases} \quad (10)$$

Where A_{sl} is the adherent force between solid and liquid surface;
$\gamma_{sv} = \gamma_s$ is the surface tension force between solid and vapor surface;
$\gamma_{lv} = \gamma$ is the surface tension force between liquid and vapor surface;
γ_{sl} is the surface tension force between solid and liquid surface.

The quadruple parameters $(\gamma_{sv},\ \gamma_{lv},\ \gamma_{sl}, \text{and}\ \ \theta)$ are difficult to experimentally identify. Lie and Neumann [17] proposed a state equation that can be used with several liquid drop volumes and their profile to determine these parameters by assuming that $\gamma_{sv} = \gamma_s$ is constant for an identical solid surface and that $\gamma_{lv} = \gamma$ is constant for an identical liquid in the same environment. The state equation can be written as follows:

$$\gamma(1 + \cos(\theta)) = 2\sqrt{\gamma\gamma_s}\exp(-\beta(\gamma - \gamma_s)) \quad (11)$$

Where β is a constant related to the volume of the liquid drop.

From the state equation, a procedure is proposed to calibrate β and determine the contact angle θ:

- For any given γ, θ and β, γ_s can be determined:

$$residual = \left|\gamma(1 + \cos(\theta)) - 2\sqrt{\gamma\gamma_s}\exp(-\beta(\gamma - \gamma_s))\right| \quad (12a)$$

$$\gamma_s^* = argmin_{\gamma_s}\left(\left|\gamma(1 + \cos(\theta)) - 2\sqrt{\gamma\gamma_s}\exp(-\beta(\gamma - \gamma_s))\right|\right) \quad (12b)$$

- As we can accurately evaluate the section area of a weld bead, β is supposed to be expressed as a function of the area section A:

$$\beta = CA \quad (13)$$

Where C is a constant;

- Based on a 2D experimental profile, A_1 and θ_1 can be measured. Then, for any chosen value of $\beta = \beta_1$, the area section can be expressed:

$$\beta = \beta_1 \frac{A}{A_1} \quad (14)$$

- Thus, equation (12) can be re-written as:

$$\theta(A,\beta_1) = \arccos\left(2\sqrt{\frac{\gamma_s(\beta_1)}{\gamma}}\exp\left(-\beta_1\frac{A}{A_1}(\gamma-\gamma_s(\beta_1))\right)-1\right) \quad (15)$$

- Another experimental profile is needed to calibrate β_1. Let's assume that A_2 and θ_2 are measured by a second 2D experimental profile. β_1 can be determined by:

$$\beta_1^* = argmin_{\beta_1}(|\theta(A_2,\beta_1)-\theta_2|) \quad (16)$$

- Hence, we can determine the contact angle as function of the section area A as follows:

$$\theta(A) = \arccos\left(2\sqrt{\frac{\gamma_s^*(\beta_1^*)}{\gamma}}\exp\left(-\beta_1^*\frac{A}{A_1}(\gamma-\gamma_s^*(\beta_1^*))\right)-1\right) \quad (17)$$

With different process parameters, the manufacturing of different weld beads is carried out. The power source model is used to compute the wire speed in order to properly estimate the area section. The discussion in the following section details numerically the above proposed procedure to determine the contact angle by the state equation of Lie-Neumann in order to validate the simulated contact angle vs the experimental one.

3 RESULTS AND DISCUSSIONS

3.1 Calibration and validation of power generator model

In this section, the fusion flow constant parameters C_1 and C_2 of the power generator model is calibrated with the mean value of the measured wire speed of $CT = 15mm$ (blue line as illustrated in fig. 8). Then, with these calibrated values, the power generator model is used to simulate the wire speed in order to validate the results according to mean values of the measured wire speed of $CT = 10mm$ and $20mm$. Table 3 indicates the synergy parameters used in the power generator.

Table 3: Parameters for the power generator.

$V_{oc}(V)$	$ws(m/s)$	$r_w(mm)$
17.2	0.133	0.5

Using the calibration method as indicated in the section 2.1, table 4 shows the values of the fusion flow constant parameters calibrated for $CT = 15mm$.

Table 4: Calibrated value of the fusion flow constant parameters.

$C_1(\times 10^{-11})$	$C_2(\times 10^{-11})$
9.6	87

Table 5 displays the comparison between the experimental wire speed and the simulated one. The maximum error is under 5%. It shows a good agreement between the experimental and simulated wire speeds.

The power generator model is used in the following section with given process parameters in order to estimate the weld bead area section considering the solidification shrinkage.

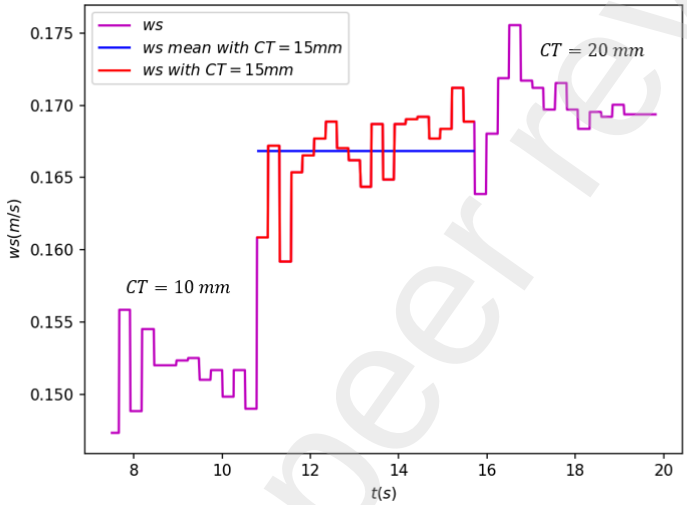

Figure 8: Evolution of the wire speed of the three parts of the weld bead.

Table 5: Comparison of the simulated and measured wire speed.

$CT(mm)$	$ws_{meas}(m/s)$	$ws_{sim}(m/s)$	$err.rela(\%)$
15	0.166	0.166	0
10	0.151	0.155	2.9
20	0.169	0.178	4.8

3.2 Weld bead simulation for inclined plane

This section is dedicated to the validation of contact angles (advance and recession) of weld bead model on an inclined plane and by comparison to experimental measures. The inclined angles of 5.47°, 12.5°, 25.6°, 33.9°, and 44.2° are chosen to manufacture the weld beads.

Fig. 9 (a) and (b) illustrate the measured advance and recession contact angle of a weld bead on the inclined plane of 33.9°. Fig. 10 (a) depicts the evolution of surface tension and the gravity

force as a function of the Laplace contact angle. At the intersection of the two forces, the critical Laplace contact angle can be determined, then the advance and recession contact angles are estimated.

Fig. 10 (b) shows the simulated weld bead profile and the computed advance and recession contact angles. The simulated contact angles are close to the measurement one with a maximum error of 0.6°.

Table 6 displays the comparison between the advance and recession contact angles of different inclined angles. The maximum error is around 2°. The larger is the inclined angle, the smaller is the error. Globally, the simulated contact angles are in good agreement with the experimental ones.

When the inclined angle increases, the gravity force in the direction of the inclined plan also increases. The balance of forces could possibly not reach its equilibrium. The weld bead on 65° inclined plane is simulated. The advance and recession contact angles are estimated around 99.5° and 79.5° respectively. Fig. 11 (a) shows the weld bead profile on the inclined plane such that at 66°, the force balance cannot reach its equilibrium. This angle is considered as the critical angle for a weld bead deposition with a given volume.

When the inclined angle decreases the gravity force along the inclined plane decreases. The capillary force also decreases because the hysteretic contact angle becomes smaller. The divergence of the resolution algorithm of equations (9) is observed due to the balance of forces. The optimal critical contact angle cannot be determined. At the inclined angle of 1°, we can simulate the weld bead profile as shown in fig. 11 (b). The advance and recession contact angles are estimated around 60.6° and 61.1° respectively.

The weld bead topology model on 1° angle inclined plane is simulated with different process parameters to simulate contact angles. The angles are used to compare with the angles simulated by the state equation which is described in the next section.

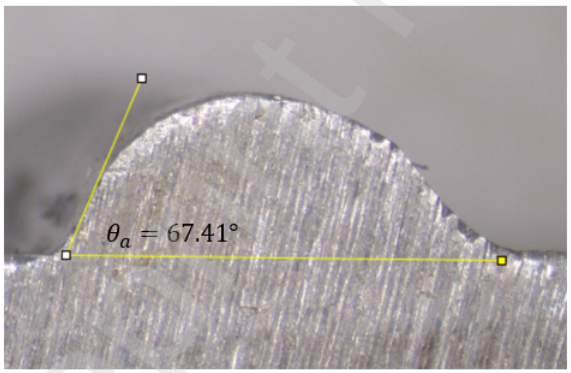

(a)

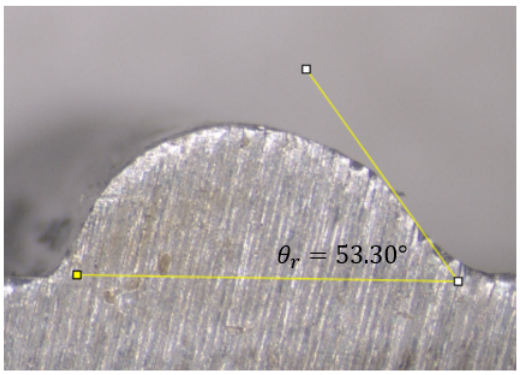

(b)

Figure 9: Measure of the advance (a) and recession (b) contact angle of a weld bead on the inclined plane of 33.9°.

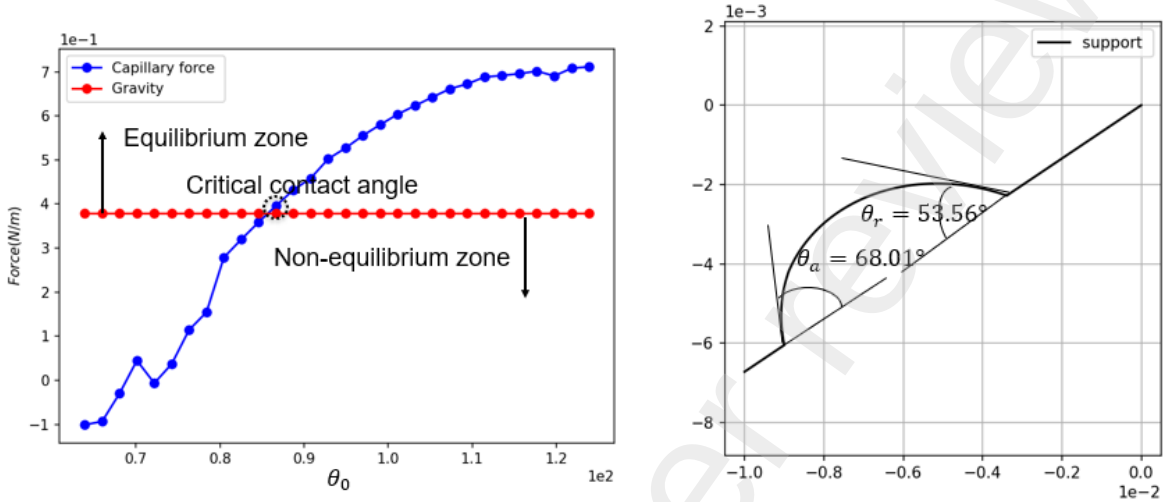

(a) (b)

Figure 10: (a) Evolution of the gravity and capillary forces as function of contact angle. (b) Simulation results

Table 6: Comparison of the measured, and simulated advance and recession contact angles for different slopes.

$\alpha(°)$	$\theta_{a,meas}(°)$	$\theta_{r,meas}(°)$	$\theta_{a,sim}(°)$	$\theta_{r,sim}(°)$
5.47	58.34	55.08	60.32	57.81
12.5	62.27	54.23	62.46	56.72
25.6	65.93	53.45	65.18	54.00
33.9	67.41	53.30	68.01	53.56
44.2	71.23	54.57	71.54	54.15

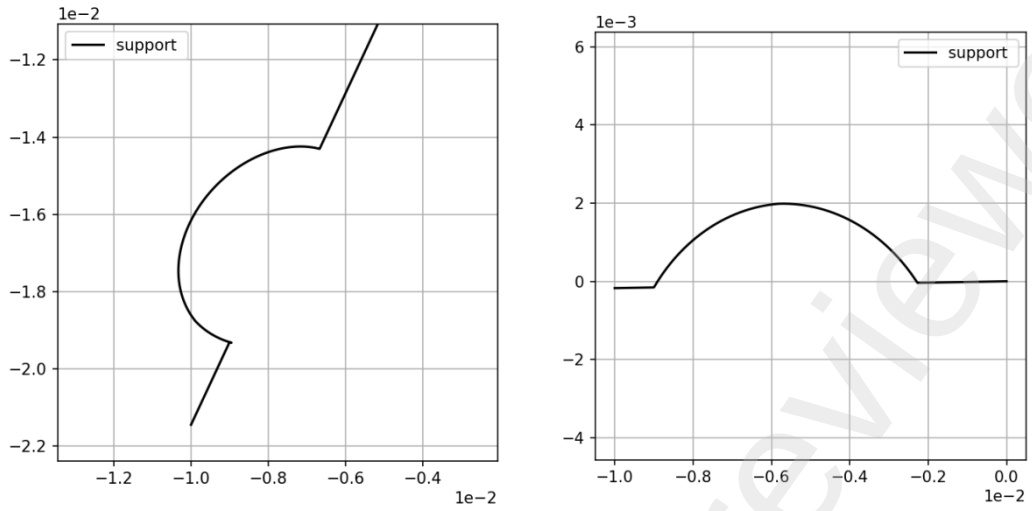

(a) (b)

Figure 11: Weld bead profile for the inclined angle (a) 65° and (b) 1°.

3.3 Weld bead simulation for horizontal plane

This section describes the procedure for computing the contact angle of a weld bead deposed on a horizontal plane as well as the validation of the model. The process parameters are used as indicated in the power generator section. The torch speed values considered are 0.5, 0.75, 1., 1.25, and 1.5 m/min. The change in torch speed induces the change in deposed volume as well as the area section of the weld bead. Using power generator model with shrinkage value, we can estimate the area section of the weld bead as displayed in the following table:

Table 7: Estimated area section of the weld beads with different torch speeds.

$v_r(m/min)$	1.5	1.25	1.	0.75	0.5
$A(\times 10^{-6}m^2)$	4.9	6.1	7.4	9.7	14.2

Fig. 12 illustrates the evolution of the residual curves of the state equation (equation 12a) for $\beta_0 = 0.25$ and $\beta'_0 = 1.$ as function of the surface tension force between solid and vapor γ_s with $v_r = 1.5m/min$ corresponding to the measured contact angle $\theta_0 = 50.8°$ and estimated area section $A_0 = 4.9 \times 10^{-6}m^2$. The curves show that there is a unique minimum value of γ_s.

Fig. 13 displays the evolution of minimum value of γ_s in function of β for a fixed $\theta_0 = 50.8°$. The curve shows that $\gamma_s(\beta)$ is monotonously increased.

Two experimental profiles are used for calibrating the state equation's parameter β. The contact angles and section areas of the profiles are $(\theta_0 = 50.8°, A_0 = 4.9 \times 10^{-6}m^2)$ and

$(\theta_1 = 56.9°, A_1 = 7.4 \times 10^{-6} m^2)$ respectively. Fig. 14a shows the evolution of $\gamma_s(\theta)$ with an initial parameter $\beta_0 = 1.5$. In this case, we obtain $\beta_1 = 2.25, \gamma_s = 1.65\ N/m$ and estimated contact angle $\tilde{\theta}_1 = 60.33°$. Using equation 15 and 16, we can find the optimal parameter $\beta'_0 = 0.25$. In this case, we obtain $\beta_1' = 0.377, \gamma_s' = 1.437\ N/m$ and estimated contact angle $\tilde{\theta}_1' \approx \theta_1 = 56.9°$. Fig. 14b displays $\gamma_s(\theta)$ at which the parameter β_0 is calibrated. The values of $(\beta_0,\ \gamma_s)$ are used to estimate the contact angle for different values of section area by equation 17. Fig. 15 shows that the contact angles with different values of section area are obtained by the intersection of black line and different curves of $\gamma_s(\theta)$.

On the other hand, we employ the topology model of weld bead on the inclined plane of angle 1° to determine the contact angle. Table 8 resumes the estimation of the contact angles of the weld beads on the horizontal plane with the two methods with different area sections. The simulated contact angle with the topology model of the weld bead on an inclined plane generates large errors for the smaller and larger estimated area sections of the weld bead. However, the simulated contact angles by the state equation well estimate the measured contact angles. The maximum error is around 3°.

Fig. 16 depicts the simulated profiles using contact angles obtained by the state equation resolution compared to the experimental ones for $(a)\ v_r = 0.5\ m/min$, $(b)\ v_r = 0.75\ m/min$, $(c)\ v_r = 1.m/min$, and $(d)\ v_r = 1.5\ m/min$. One can employ the state equation and Laplace equation to simulate different process parameters by coupling with power generator model for weld bead deposition on the horizontal plane.

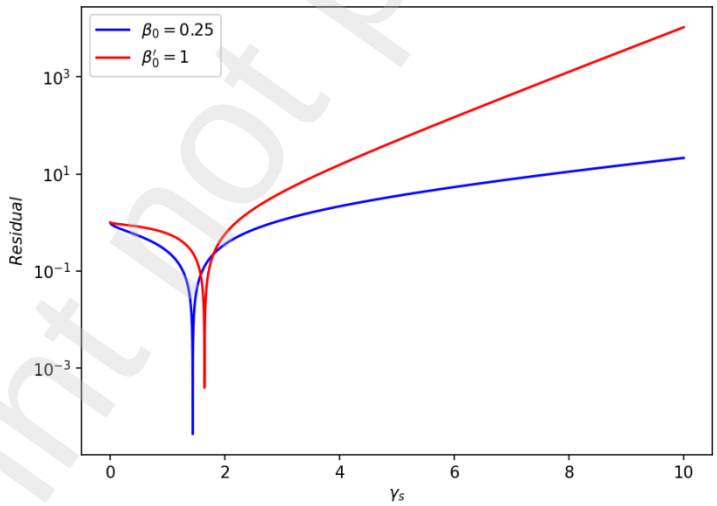

Figure 12: Evolution of the residual of the state equation for two different values of weld bead volume-related parameters β.

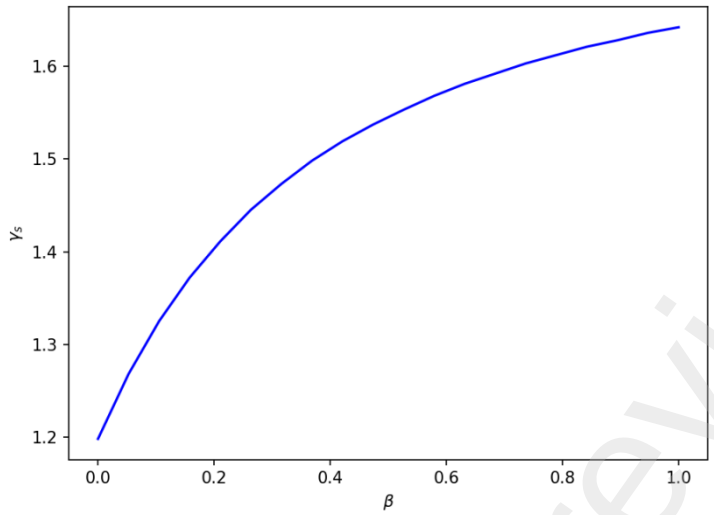

Figure 13: Evolution of surface tension force between the solid-vapor surface in function weld bead volume-related parameters.

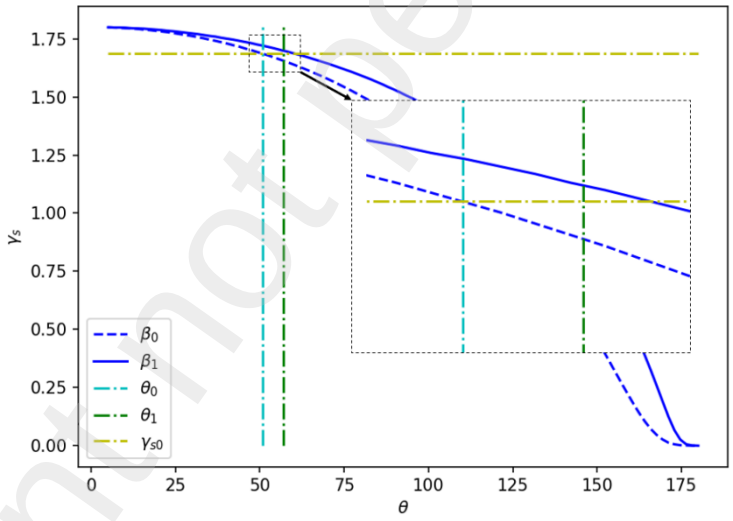

(a)

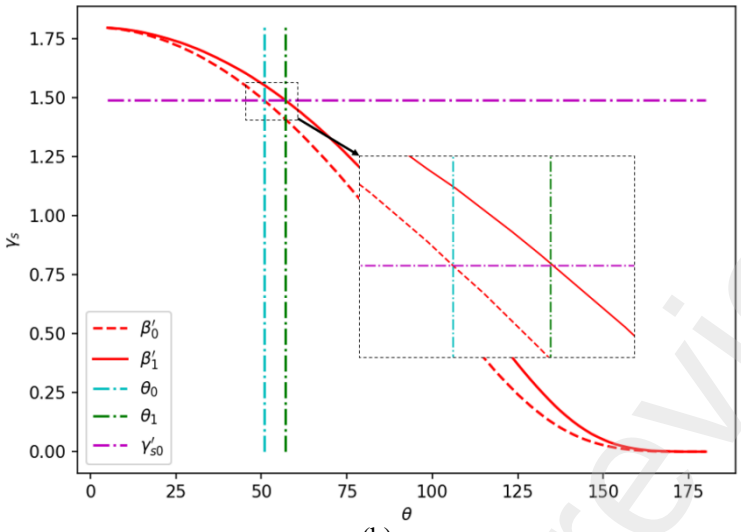

(b)

Figure 14: γ_s curves as function of contact angle and calibration of β_0 with θ_0 and targeted contact angle θ_1 (a) initial value and (b) calibrated value.

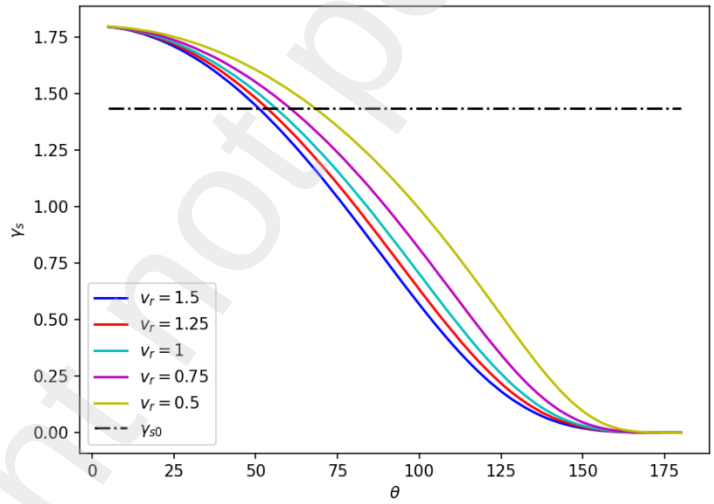

Figure 15: Evolution of γ_s curves with different process parameters and contact angle estimation with γ_s^0 from the β_0 calibrated.

Table 8: Comparison of the measured contact angles and the simulated ones by 1° inclined angle topology model and state equation.

$Area\ (\times 10^{-6}m^2)$	$\theta_{meas}(°)$	$\theta_{sim,\,inclined}(°)$	$\theta_{sim,\,state-eqn.}(°)$
4.9	50.8	45.15	50.80
6.1	51.1	50.5	53.29
7.4	56.9	54.1	56.90
9.7	57.9	60.3	60.32
14.2	64.3	74.15	67.81

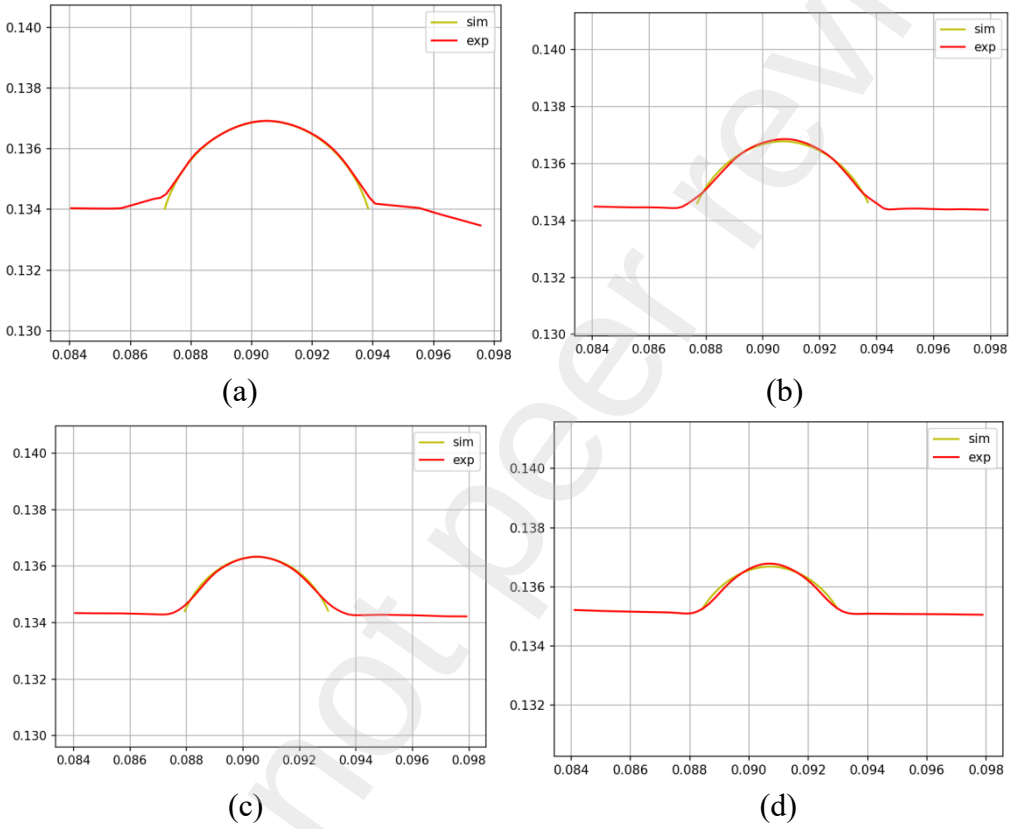

Figure 16: Comparison of the experiment and simulated weld bead profiles with contact angles computed by state equation for different torch speeds (a) 0.5 m/min, (b) 0.75 m/min, (c) 1. m/min, and (d) 1.5 m/min.

4 CONCLUSIONS

A methodology using a power generator model to couple with a physical topology model has been introduced to simulate the topology of a deposed weld bead on an inclined or a horizontal plane. The description of a simplified power generator model has been detailed. The fusion molten flow constant parameters need to be calibrated with the measured wire-speed for a given process parameter. The simulated wire speed is in good agreement with the measured one for different values of CT. The power generator model is used to simulate the wire speed to estimate the section area from the conservation of the flow. However, according to the large

temperature gradient the solidification shrinkage occurs. A method to approximate the shrinkage value for this study has been demonstrated to estimate correctly the area section of a deposed weld bead.

In addition, a method for accurate estimation of contact angle has also been presented to determine the contact angle from the experimental profiles as well as the simulated ones in order to validate the simulated contact angle by the physical topology model.

On an inclined plane, we have proposed a simplified physical model to simulate the 2D topology of a weld bead using the Laplace equation and the capillary-gravity force equilibrium. Step by step resolution method is proposed to solve the proposed system of physical equations. Moreover, on a horizontal plane, the state equation of Lie-Neumann is used to determine the contact angle. The experimental validation of the weld bead profiles and contact angles for both cases (weld bead topology on an inclined and a horizontal plane) has been performed.

Using this physical weld bead topology model coupling with a power generator model, one can depose a weld bead with different process parameters on an inclined or a horizontal plane. We need to extend the work to find a simplified model able to simulate a weld bead profile deposed on any substrate.

ACKNOWLEDGEMENTS

The authors would like to thank the industrial partners of the AFH [18] (Additive Factory Hub) consortium for their support in the framework of the WAS project. This project is as well supported by the French government's aid in the framework of PIA (Programme d'Investissement d'Avenir) for Institut de Recherche Technologique SystemX.

REFERENCES

[1] https ://www.irt-systemx.fr/projets/was/
[2] De Gennes, P.G., Wyart, F.B., and Quéré, D. *Gouttes, bulles, perles et ondes.* Belin (2002).
[3] Sánchez-Balderas, G., Pérez, E. *On the usefulness of the equation of state approach for contact angles on rough surfaces*. Appl. Phys. A 126, 20 (2020).
[4] Golob, M. *Modelling and Simulation of GMA Welding Process and Welding Power Sources.* Simul. Notes Eur. **26(4):** 237-244 (2016).
[5] Frazier, W.E. *Metal additive manufacturing: a review*. J. Mater Eng. Perform **23(6):** 1917–1928 (2014).
[6] Jones, L.A., Eagar, T.W., and Lang., J.H. *A dynamic model of drops detaching from a gas metal arc welding electrode*, J. Phys. Appl. Phys., **31(1):**107-123 (1998).
[7] Robert, P., Museau, M. and Paris, H. *Effect of Temperature on the Quality of Welding Beads Deposited with CMT Technology*, *International Conference on Industrial Engineering and Engineering Management (IEEM)*, 680-684 (2018).
[8] Mohebbi, M.S., Kühl, M. & Ploshikhin, V. *A thermo-capillary-gravity model for geometrical analysis of single-bead wire and arc additive manufacturing (WAAM). Int J Adv Manuf Technol* **109:**877–891 (2020).
[9] Wu, D., Wang, P., Wu, P., Yang, Q., Liu, F., Han, Y., Xu, F., and Wang, L. *Determination of contact*

angle of droplet on convex and concave spherical surfaces, Chem. Phys., **457:** 63-69 (2015).

[10] Quéré, D., Azzopardi, M.J, and Delattre, L. Drops *at Rest on a Tilted Plane*, Langmuir ***14*** **(8):**2213-2216 (1998).
[11] Fronius, «CMT». https://www.fronius.com/fr-fr/france.
[12] Naidu, D.S., Ozcelik, S. and Moore, K.L. *Modeling, sensing and control of gas metal arc welding,* Mod., Sens. and Cont. of GMAW. 1-351 (2003).
[13] Sindo, K., *Welding metallurgy*, New Jersey, USA 431–446 (2003).
[14] Albert, E., Tegze, B., Hajnal, Z., Zámbó, D., Szekrényes, D.P., Deák, A., Hórvölgyi, Z. and Nagy, N. *Robust Contact Angle Determination for Needle-in-Drop Type Measurements,* ACS Omega **4(19):**18465-18471 (2019).
[15] Saecfr, C.M. and Ash, E.J. *A method for determining the volume changes occurring in metals during casting*, J. American Soc. For Nav. Eng., **44(2):**271-272 (1932).
[16] TWI (The Welding Institute), https://www.twi-global.com/technical-knowledge/job-knowledge/distortion-types-and-causes-033.
[17] Li, D. and Neumann, A., J. *Colloid Interface*, Sci. **137(1):**304 (1990).
[18] https://www.additivefactoryhub.com/